Materials & Design 205 (2021) 109699

Contents lists available at ScienceDirect

Materials & Design

journal homepage: www.elsevier.com/locate/matdes

4D printing of highly printable and shape morphing hydrogels composed of alginate and methylcellulose

Jiahui Lai [a,1], Xinliang Ye [b,1], Jia Liu [c,1], Chong Wang [b,*], Junzhi Li [a], Xiang Wang [b], Mingze Ma [d], Min Wang [a,*]

[a] Department of Mechanical Engineering, The University of Hong Kong, Pokfulam Road, Hong Kong Special Administrative Region
[b] School of Mechanical Engineering, Dongguan University of Technology, Songshan Lake, Dongguan, PR China
[c] Department of Orthopaedics, Affiliated Hospital of Youjiang Medical University for Nationalities, Baise, Guangxi, PR China
[d] Guangdong Key Laboratory for Biomedical Measurements and Ultrasound Imaging, Health Science Center, Shenzhen University, Shenzhen, Guangdong, PR China

HIGHLIGHTS

- A versatile strategy to develop shape morphing hydrogel with swelling anisotropy.
- The use of single ink to create heterogeneous structures without using chemical reactions.
- Excellent printability of the shape morphing hydrogel.
- Ability to print out a series of simple and complex dynamic structures with high accuracy.
- Relatively fast shape morphing process within just a few minutes.

GRAPHICAL ABSTRACT

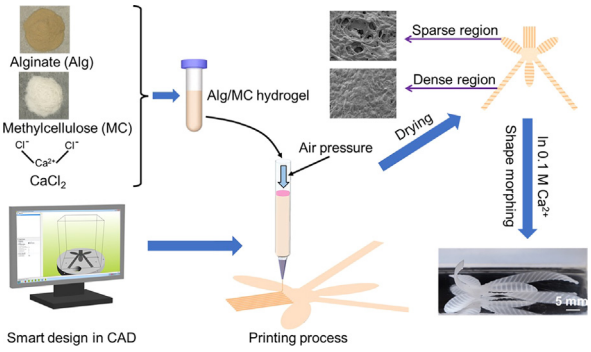

ARTICLE INFO

Article history:
Received 15 January 2021
Revised 1 March 2021
Accepted 30 March 2021
Available online 6 April 2021

Keywords:
4D printing
Shape morphing hydrogel
Excellent printability
Alginate and methylcellulose

ABSTRACT

4D printing of swellable/shrinkable hydrogels has been viewed as an appealing approach for fabricating dynamic structures for various biomedical applications. However, 4D printing of precise hydrogel structures is still highly challenging due to the relatively poor printability of hydrogels and high surface roughness of printed patterns, when micro extrusion-based 3D printers are used. In this study, a highly printable and shape morphing hydrogel was investigated for 4D printing by blending alginate (Alg) and methylcellulose (MC). The optimized Alg/MC hydrogel exhibited excellent rheological properties, extrudability and shape fidelity of printed structures. The printable Alg/MC hydrogel was 4D printed into a series of patterned 2D architectures which were encoded with anisotropic stiffness and swelling behaviors by strategically controlling the network density gradients vertical to the orientation of the patterned strips. By controlling the strip interspacing and angle, these 2D architectures could transform into various prescribed simple 3D morphologies (e.g., tube-curling and helix) and complex 3D morphologies (e.g., double helix and flowers) after immersion in a calcium chloride solution. This shape morphing Alg/MC hydrogel with excellent printability has high potential for 4D printing of delicate hydrogel patterns, which are increasingly needed in the tissue engineering, biomedical device and soft robotics fields.

1. Introduction

Four-dimensional (4D) printing has attracted increasing attention since its proposal in 2013 by Tibbits at the Self-Assembly Lab of MIT. This advanced technique enables us to fabricate dynamic structures which can change their shapes, functions or

* Corresponding authors at: School of Mechanical Engineering, Dongguan University of Technology, 1 Daxue Road, Songshan Lake, Dongguan, PR China (C. Wang); Department of Mechanical Engineering, The University of Hong Kong, Pokfulam Road, Hong Kong, Hong Kong SAR, PR China (M. Wang).
E-mail addresses: wangchong@dgut.edu.cn (C. Wang), memwang@hku.hk (M. Wang).
[1] These authors contributed equally.

https://doi.org/10.1016/j.matdes.2021.109699
0264-1275/

properties along with time when appropriate external stimuli (e.g., water, pH, temperature) are applied. There are a number of technologies being developed for 4D printing such as micro extrusion-based 3D printing [1,2], fused deposition modeling [3], stereolithography [4] and digital light projection [5]. Among them, micro extrusion-based 3D printing is one of the most commonly used 4D printing technologies due to its ease of operation and ability to process a variety of ink materials.

Smart materials and smart design are two key components in 4D printing to achieve stimuli-responsive behavior. Smart materials are materials that can change their shape and properties under appropriate stimuli [6]. Smart design is the design that is pre-programmed carefully in CAD by fully taking into account any anticipated time-dependent deformations of the 4D printed objects [7]. Since 4D printing is still at the stage of early development, currently available smart materials are limited and most of them are shape memory polymers (SMPs) and hydrogels. SMPs are those polymers that can fix a temporary shape and recover their permanent shape upon external stimuli, such as heat, light [8]. A number of SMPs have been explored for 4D printing in biomedical engineering such as poly(lactic acid) [3], polyurethane [9], poly(D,L-lactide-*co*-trimethylene carbonate) [10,11], methacrylated polycaprolactone [4]. In addition to SMPs, hydrogels are another type of appealing material for 4D printing in biomedical applications. Hydrogels exhibit swelling/shrinking behavior when solvent molecules enter/leave the polymer networks. By smartly controlling the swelling/shrinking rates or degrees, hydrogels can change the volumes sizably and anisotropically, making it possible to fabricate hydrogel architectures with the ability of programmed shape transformation via 4D printing. For example, gelatin methacryloyl (GelMA) and hyaluronic acid methacryloyl have been 4D printed into self-folding scaffolds for tissue engineering by controlling the photo crosslinking degree gradients across the thickness of the hydrogels [2,12]. Hydrogels doped with oriented fibers exhibited anisotropic stiffness and swelling and hence have been used to fabricate different shape morphing structures [13]. However, most of the hydrogels used in 4D printing exhibit poor printability and are challenging for printing complex structures with high precision to achieve the smart design of 4D printing and hence desirable shape morphing process.

The printability of hydrogels subjected to micro extrusion-based 4D printing is primarily dependent on their rheological properties [14,15]. The important rheological parameters that affect the printability of a hydrogel are viscosity, shear thinning and thixotropy. A printable hydrogel should be highly viscose and exhibit good shear thinning behavior and high thixotropic property. High viscosity enables hydrogels remaining static before printing. Good shear thinning behavior enables hydrogels to greatly decrease the viscosity when subjected to a shear force (determined by extrusion parameters such as nozzle size and applied printing pressure) and to pass through a nozzle smoothly during printing. High thixotropic property enables quick self-recovery of hydrogels to support the already printed part when a shear force is removed after printing. Besides, a printed structure should keep a good shape fidelity which is a direct indication for a good printability.

Alginate (Alg) hydrogel has been widely used for 3D printing for tissue engineering due to its excellent biocompatibility, low toxicity, relatively low cost and rapid gelation in the presence of Ca^{2+} divalent cation [16,17]. However, 4D printing of alginate hydrogel is rarely reported due to the poor printability and limited shape morphing ability. When alginate is mixed with another polymer, such as polydopamine [18], an Alg-based blend hydrogel with desired shape morphing ability and printability may be obtained. Methylcellulose (MC) is a chemically modified cellulose that has been widely used as a viscosity enhancer for food industry and pharmaceutics. Therefore, adding MC to an alginate hydrogel could greatly improve its viscosity and hence printability [19]. Besides, the addition of MC polymer still maintains the polymer network of the alginate [20,21]. Therefore, by smartly controlling the difference of network density across the Alg/MC hydrogel, it is possible to obtain swelling anisotropy and shape morphing ability for 4D printing.

In this study, we demonstrated a facile and robust strategy to integrate shape morphing ability into the highly printable Alg/MC blend hydrogel for 4D printing. This strategy is based on controlling the network density gradient across the Alg/MC hydrogel plane, leading to anisotropic stiffness and swelling, and finally resulting in programmed deformation of the Alg/MC hydrogels by responding to calcium chloride ($CaCl_2$) solution. Using this strategy, Alg/MC hydrogel inks with good printability were 4D printed into a series of simple and complex patterned architectures which could change shape on immersion in $CaCl_2$ solution, yielding simple and complex 3D morphologies. This strategy used single Alg/MC hydrogel to create heterogeneous dynamic constructs without involving chemical reactions, which is rarely reported in other 4D printing researches. Overall, the feasibility of Alg/MC blend hydrogel as a novel smart material for 4D printing was investigated in terms of its printability and shape morphing abilities.

2. Materials and methods

2.1. Materials

Sodium alginate and methylcellulose (MW = ~88 kDa) were purchased from Sigma-Aldrich, Hong Kong. Calcium chloride was obtained from Uni Chem Co., LTD., Korea. All reagents were directly used in the experiments without further purification. Deionized (DI) water, obtained from a DI water machine (Model D12681, Barnstead International), was used in all the experiments.

2.2. Hydrogel preparation

To prepare Alg/MC hydrogels with different MC concentration, firstly a certain amount of Alg powder was added into a 0.075% (w/v) $CaCl_2$ solution and magnetically stirred overnight at 40 °C to obtain a homogeneous pre-partially crosslinked 3% (w/v) Alg hydrogel. The Alg hydrogel was then heated to about 80 °C and MC powder with different concentration of 1% (w/v), 5% (w/v) and 9% (w/v) was added, respectively, to generate Alg/MC hydrogels with different MC content. Afterwards, the mixture was magnetically stirred until the MC powder was dispersed homogeneously and at the same time the temperature of mixture was gradually cooled. Once the mixture was cooled to room temperature, the MC powder began to hydrate and resulted in the increased viscosity of the mixture. Finally, the mixture was placed at room temperature overnight to obtain Alg/MC hydrogel with full dissolution of MC. In this work, the prepared Alg/MC hydrogels with different MC concentration were referred as Alg3/MC1, Alg3/MC5 and Alg3/MC9. For comparison, 3% (w/v) Alg (Alg3), 1% (w/v) MC (MC1), 5% (w/v) MC (MC5) and 9% (w/v) MC (MC9) were prepared by adding Alg powder or MC powder into the hot 0.075% (w/v) $CaCl_2$ solution, respectively.

2.3. Printability

2.3.1. Rheology characterization

The rheology of the Alg/MC blend hydrogels with different MC content was characterized using a rotational rheometer (MCR302, Anton Paar, Austria) with a 25 mm parallel plate and 0.55 mm measurement gap. Three theological tests were performed at room temperature (the working temperature of the 3D printer): (1) shear thinning property; (2) angular frequency sweep;

(3) thixotropic characterization. For the shear thinning property, the viscosity of tested hydrogels was measured at shear rates ranging from 0.1 to 1000 s^{-1}. For the angular frequency sweep, first of all, strain sweeps from 0.1% to 100% at a frequency of 1 Hz were performed to determine the linear viscoelastic region (LVR). From the LVR, a constant strain of 1% was chosen for the angular frequency sweeps at an angular frequency range of 1–100 rad/s. For the thixotropic property, the test was performed in three steps to evaluate the recoverability of the Alg/MC hydrogels. At step I, a shear rate of 0.1 s^{-1} was applied for the hydrogels for 60 s to observe the state of hydrogels without shear force before printing. At step II, the shear rate was instantly and greatly increased and hold for 10 s to observe the sheared state of hydrogels under shear force during printing. The shear rate at this step was chosen based on the theoretical shear rates of the tested hydrogels in the nozzle, which were calculated based on a power-law model described in literature [22]. At step III, the shear rate was returned to 0.1 s^{-1} and retained for 60 s to observe the viscosity recovery of the hydrogels when removing shear force after printing.

2.3.2. Shape fidelity

To observe the shape fidelity of the Alg/MC hydrogels, a grid (20×20 mm^2, line spacing 2 mm, 1 layer) was 3D printed directly onto glass slides using a 3D bioprinter (3D Discovery™ Evolution, regenHU Ltd, Switzerland). Once the printing is finished, the shape of grids was imaged using a digital single lens mirrorless (DSLM) camera (Z6, Nikon, Japan). The strut diameter of each printed structure with grids was measured at 10 different points using the software ImageJ.

2.4. 4D printing procedure

In this work, the Alg3/MC9 hydrogel was 4D printed using the Regenhu 3D bioprinter (3D Discovery™ Evolution, regenHU Ltd, Switzerland). The air pressure was set as 2.5 to 3 bar; the layer thickness was set as 0.2 mm; the printing speed was 8 mm/s; the inner diameter of the nozzle of the printing head was 0.41 mm (22G). The hydrogel was printed onto silica slides for easy detach after drying. The 4D printing procedure is illustrated as Fig. 1. Briefly, the first step was to fabricate the 2D hydrogel patterns according to the preprogrammed CAD design which was performed in the software of BioCAD (Regenhu). Next, the patterned hydrogels were dried at room temperature for about 8 h. Finally, the dried hydrogels were immersed into a 0.1 M $CaCl_2$ solution tank, leading to 3D deformations of the 4D printed Alg3/MC9 hydrogel patterns. The 4D printed structures were a three-layered configuration where the first layer was a film with no strip interspacing while the second and third layers were the same printed pattern printed at a specific strip interspacing and angles θ. During drying, the three-layer areas of the printed structure would be fused and compressed into dense regions with a high network density, while single-layer areas of the printed structure would become relatively sparse regions with a low network density. As such, the 4D printed patterned Alg3/MC9 hydrogels generate different network densities within the architectures, leading to anisotropic swelling and hence controlled shape morphing process according to preprogrammed design. The effect of printing angle and strip interspacing on the 3D deformations of the 4D printed Alg3/MC9 architectures was studied. Thereafter, Alg3/MC9 hydrogel was 4D printed into a series of patterns that could change from 2D morphologies into diverse prescribed simple 3D morphologies (e.g., bending, rolling, helix) and complex 3D morphologies (e.g., double helix, cage-shape, flowers) by responding to $CaCl_2$ solution.

2.5. Morphological characterization

The morphology of casted Alg3, MC9, Alg3/MC9 hydrogel films and 4D printed Alg3/MC9 structures were studied using a field emission scanning electron microscope (Hitachi S4800 FEG SEM, Japan). The casted hydrogel samples were frozen at −70 °C for 12 h and then freeze-dried for 2 days, while the 4D printed hydrogel samples were dried at room temperature for about 8 h and then dried at vacuum for 2 days. Next, all the hydrogel samples were sputter-coated with a thin layer of gold. The surface morphology and cross-section views of all the hydrogel samples were imaged separately under SEM, in which the cross-sectional structures were obtained by fracturing the samples in liquid nitrogen.

2.6. Swelling ratio

The swelling ratio of the sparse part and dense part of printed Alg3/MC9 hydrogels were determined by measuring the ratio between the swelling weight (W_s) and dry weigh (W_d) of each part sample. All samples were dried at room temperature for about 8 h and then were soaked in 0.1 M $CaCl_2$ solution until reaching equilibrium swelling. The dry weight and swelling weight of each sample were recorded, and the swelling ratio of each sample was calculated by W_s/W_d.

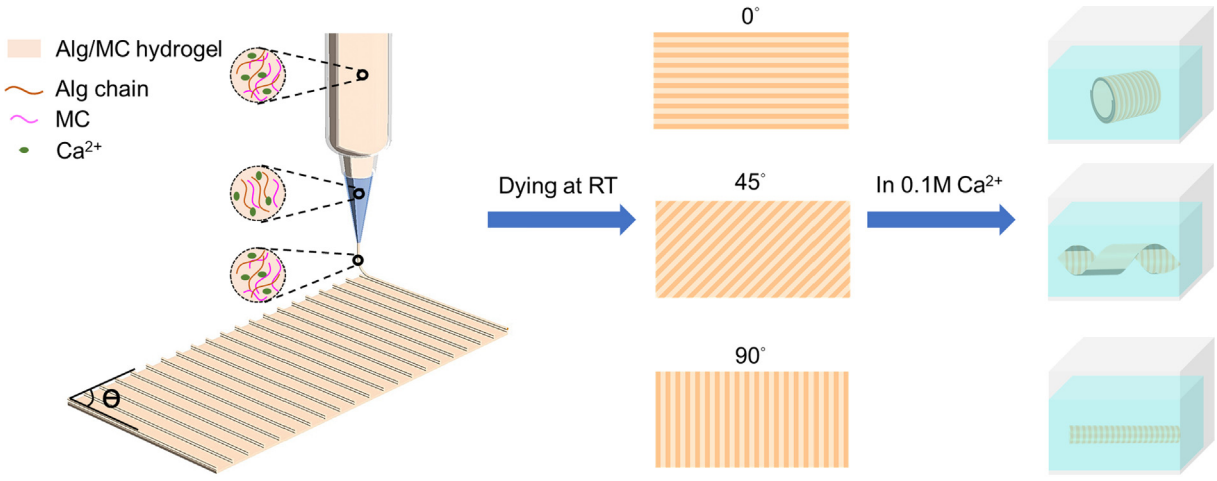

Fig. 1. Schematic illustration of 4D printing for fabrication of patterned Alg/MC hydrogels and their 3D deformations on immersion in 0.1 M $CaCl_2$ solution.

2.7. Tensile testing

The tensile testing of the sparse part and dense part of printed Alg3/MC9 hydrogels were performed using a mechanical testing machine (Instron 5848, UK) at room temperature. Briefly, the tested specimens with one-layer (i.e. sparse part) or three-layer (i.e. dense part) were firstly printed into dog bone shape with the tested region being 20 mm × 5 mm. The printed specimens were then dried at room temperature for about 8 h. After drying, the average thickness of one-layer specimens and three-layer specimens were about 0.12 mm and 0.08 mm, respectively. Before testing, the initial dimensions (width and thickness) of each tested sample were measured using a digital caliper. The specimens were hold tightly using the grippers equipped in the mechanical testing machine. The tests were performed at a constant speed of 0.5 mm/min at room temperature. Young's modulus and tensile strength were calculated based on the strain–stress curves.

2.8. Shape morphing behaviour of 4D printed patterned hydrogels

The shape morphing behaviours of all of the 4D printed patterned Alg3/MC9 hydrogels were investigated by placing the specimens in an acrylic tank containing DI water or 0.1 M $CaCl_2$ solution. The resulting shape deformation processes were recorded using the Nikon DSLM camera.

3. Results and discussion

3.1. Printability

3.1.1. Rheological properties

In rheological testing, shear thinning behavior, angular frequency sweep and thixotropic property of all the hydrogels were investigated. In the shear thinning test, as shown in Fig. 2a, it was found that the viscosity of all the hydrogel samples was decreased with the increased shear rate, demonstrating a shear thinning behavior. The shear thinning behavior of the tested hydrogels enables them to easily flow through the nozzle during printing and to form stable filaments after printing when the shear stress is released. Besides, pure Alg3 exhibited the lowest viscosity among the entire shear rate, suggesting that pure Alg had a poor printability. MC, as a viscosity enhancer, was used as a main component in the ink formulation to improve the viscosity of Alg. Interestingly, the viscosity of MC5 and Alg3/MC5 as well as MC9 and Alg3/MC9 was almost overlapping during the range of tested shear rate, indicating that the viscosity of Alg/MC blend hydrogels are mainly contributed by MC.

In the angular frequency sweep, as shown in Fig. 2b, it was found that the storage modulus G′ of Alg3, MC1 and Alg3/MC1 hydrogels was lower than the loss modulus G″, indicating that the inks were in sol-states; MC5 and Alg3/MC5 hydrogels exhibited an almost equal of G′ and G″, indicating that the inks were in sol-gel states; MC9 and Alg3/MC9 hydrogels exhibited a higher G′ than G″, indicating that the inks were in gel-states. Besides, Fig. 2c revealed the flow behaviors of different hydrogels, in which sol-like Alg3, MC1 and Alg3/MC1 hydrogels exhibited a good gravity-induced flow and the other hydrogels kept stable after inverting the hydrogel-containing tubes for 5 min.

In the thixotropic property test, the maximum shear rates of the tested hydrogels in the nozzle were firstly determined, and the results were given in Table S1. The maximum shear rates in the nozzle for low viscous Alg3, MC1 and Alg3/MC1 are higher than 2000 s^{-1}, while that for the remaining high viscous hydrogels are about 500 s^{-1} which was chosen at step II to simulate the extrusion of the hydrogels. The viscosity recovery of all the hydrogels was shown in Fig. 2d. All the hydrogels kept a stable viscosity under a low shear rate of 0.1 s^{-1} at step I, and then sharply decreased to a low viscosity under a high shear rate of 500 s^{-1} at step II, and finally recovered to a viscosity comparable to their initial value after removing the high shear rate at step III, indicating a good thixotropic properties for all the tested hydrogels. The significantly decreased viscosity of the hydrogels at step II could be attributed to the break of the enlargements or cross-links between polymer chains caused by the high shear stress. After removing the high shear stress at step III, the hydrogels can rebuild the broken cross-links after a period of rest and hence result in the increased and recovered viscosity.

3.1.2. Shape fidelity

To further confirm the printability of the Alg/MC hydrogels for micro extrusion-based printing, the shape fidelity of printed grids with a 22G nozzle was investigated. As shown in Fig. 2e, Alg3 (i), MC1 (ii) and Alg3/MC1 (iii) couldn't even maintain a grid shape of printed structures due to their too low viscosity (Fig. 2a) and liquid-like states (Fig. 2c). Although MC5 (iv) and Alg3/MC5 (v) could hold a grid shape after printing, the printed filaments showed a low resolution with an average diameter of about 1 mm (Fig. 2e(viii)) and tended to be collapse after some time. MC9 (vi) and Alg3/MC9 (vii) exhibited the best shape fidelity with a strut diameter of about 0.7 mm (Fig. 2e(viii)) and could maintain their structures stably after printing. Considering the rheological properties, shape fidelity and crosslinking ability of all the tested hydrogels, Alg3/MC9 was chosen as the best candidate to achieve the smart design of 4D printing.

For micro extrusion-based 3D printing, the printing resolution is affected by the nozzle size. The strut diameters of Alg3/MC9 hydrogel printed with a 22G nozzle and a 27G nozzle was compared (Fig. S2). It was found that the strut diameter printed with a 27G nozzle showed a higher resolution of about 0.4 mm than that (0.7 mm) printed with a 22G nozzle. However, the printing speed with a 27G nozzle was 3 mm/s, which was much slower than 8 mm/s of a 22G nozzle. Considering the printing efficiency and wide use of the 22G nozzle in various 3D printing studies [1,11], the 22G nozzle was chosen in this study for 4D printing.

3.2. 4D printing of the shape morphing Alg3/MC9 hydrogel

3.2.1. Fabrication of simple patterned hydrogels and their deformations

In recent years, a variety of approaches have been developed for preparing shape morphing hydrogels. Normally, the shape morphing ability of hydrogels are based on the nonuniformed internal stress which is induced by the uneven swelling/shrinking of different parts within a hydrogel sample. The shape morphing hydrogels with heterogeneous swelling/shrinking can be prepared with different components across the hydrogel thickness [12], or with different components across the hydrogel plane [23], or with different components across both the thickness and plane of a hydrogel sample [24]. In this work, the Alg3/MC9 hydrogel with different distributive components (i.e., different network density) in plane was prepared. The in-plane force of the hydrogel could induce curvature under suitable external stimuli and the curvature degree and direction can be adjusted by controlling the strip interspacing and angle in the hydrogels [23,24]. Therefore, a series of simple three-layer patterns with different strip interspacing and angle were printed, in order to explore differences in their shape morphing behavior on immersion in water or 0.1 M $CaCl_2$ solution.

The shape morphing degree was dependent on the printed strip interspacing, as shown in Fig. S3. The spacing between the strips has an effect on the elastic tensors and hence on the shape morphing degree [24]. When there was no strip interspacing in the three-

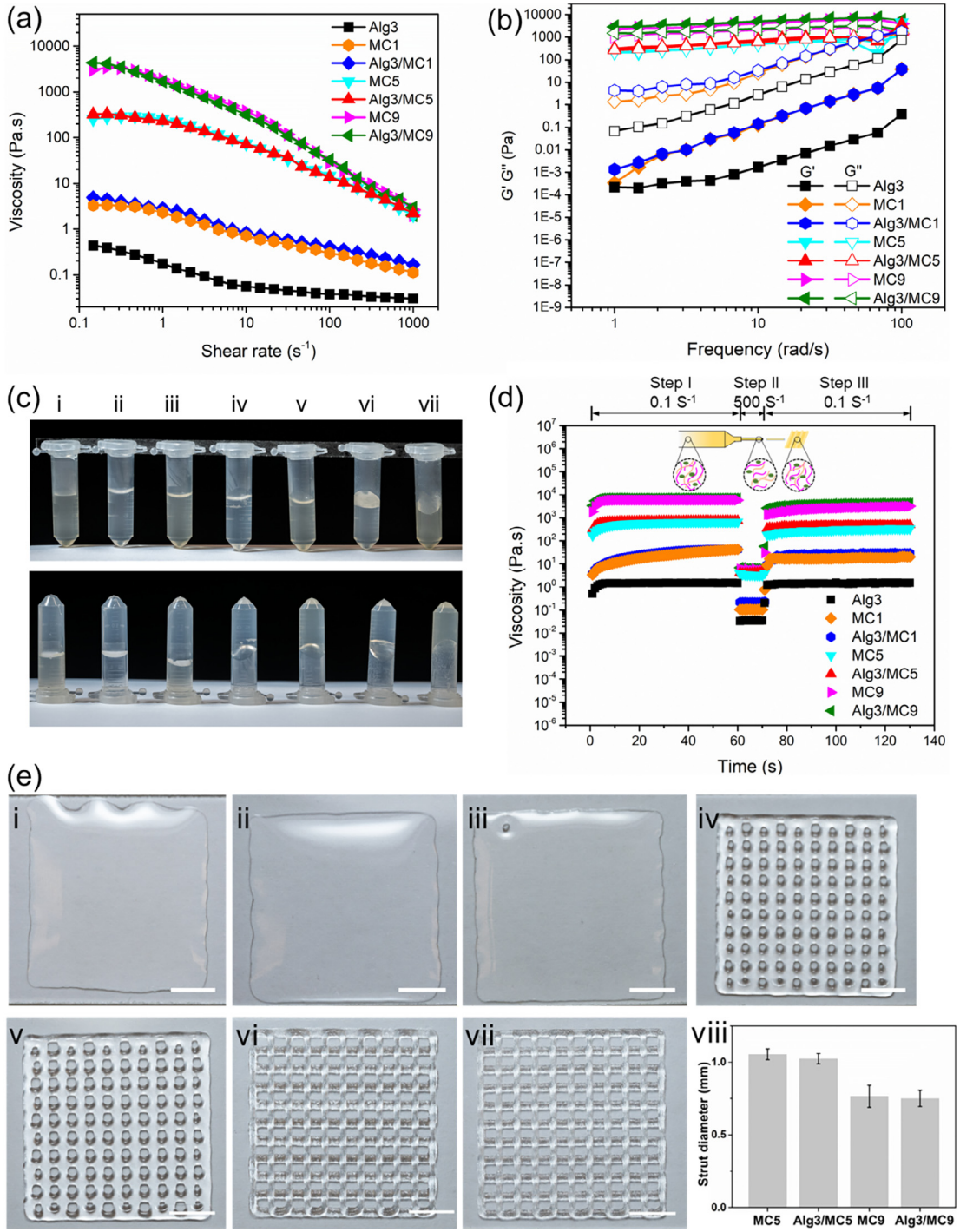

Fig. 2. Printability of Alg3 (i), MC1 (ii), Alg3/MC1 (iii), MC5 (iv), Alg3/MC5 (v), MC9 (vi), Alg3/MC9 (vii): (a) shear viscosity as a function of shear rate at room temperature; (b) storage modulus (G′) and loss modulus (G′ ′) as a function of frequency at room temperature; (c) flow behavior of each hydrogel; (d) thixotropic property; (e) photographs of the printed grids (i-vii) and their corresponding strut diameters (viii) (Scale bar: 5 mm).

layer patterns, the patterned hydrogels showed little shape deformation. Increasing strip width from 0 to 2 mm resulted in an increased bending degree of the resultant rolling structures. However, further increasing the strip width larger than 5 mm reversely decreased the bending degree.

The shape morphing direction of the patterned hydrogels can be programmed via printing the strips at a specific angle (Fig. 3 and Fig. S4). With the strips printed at the angle of 0°, 45° and 90°, the Alg3/MC9 hydrogel sheets were deformed into a tube-curling structure, a helical structure and a rolling structure, respectively (Fig. 3, Movie S1, S2 and S3). Besides, the shape morphing direction was vertical to the orientation of the printed strips. Interestingly, the resultant shape morphing morphologies showed no significant difference in the 0.1 M $CaCl_2$ solution (Fig. 3a-c) and in the DI water (Fig. 3d-f), due to no significant changes in osmotic pressure. However, the swelling Alg3/MC9 structures without crosslinking in the DI water are very weak and the transformed 3D morphologies are easily collapsed even with a little external disturbance. The cross-

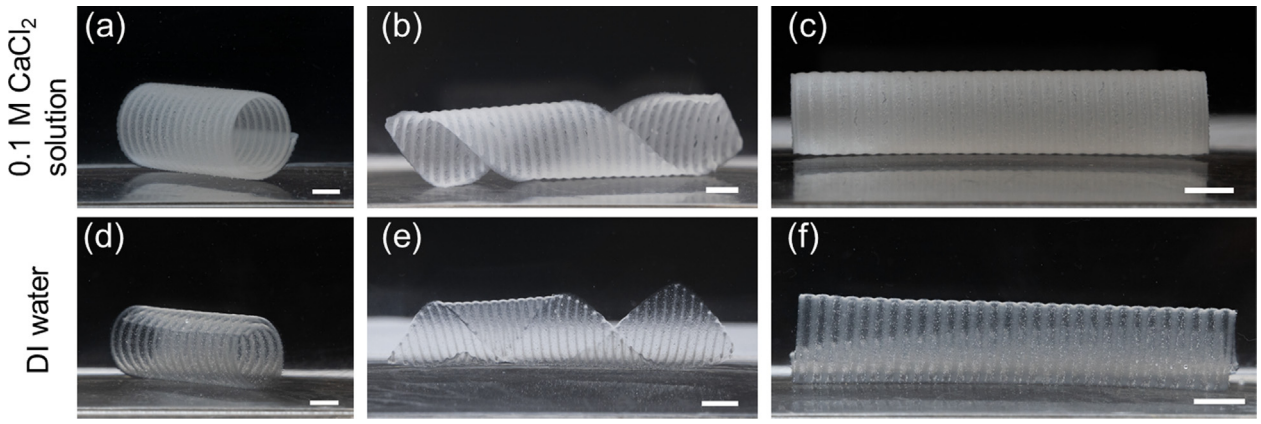

Fig. 3. 3D shape deformations of 4D printed simple patterned hydrogels with tube-curling structures, helix structures and rolling structures in the 0.1 M $CaCl_2$ solution and DI water, respectively, with well-aligned strips (line spacing: 1.4 mm) at angle = 0° (a, d), 45° (b, e), and 90° (c, f) correspondingly (Scale bar: 5 mm).

linked Alg3/MC9 hydrogels exhibited a mechanical modulus and strength at kPa scale (Fig. S1), which is sufficient to keep the structures stable. Therefore, 0.1 M $CaCl_2$ solution was chosen as external stimuli for further experiments.

Based on the relationships between the curvature degree and strips interspacing, as well as the spiral angle and printing direction, we can design hydrogel patterns for targeted shape morphing structures. Besides, these relationships could be useful to predict 4D response when a specific Alg3/MC9 hydrogel pattern is given.

3.2.2. Mechanism of the shape morphing behavior

To understand the mechanism of the shape morphing behavior of the 4D printed Alg3/MC9 hydrogels, firstly the surface morphology of the casted Alg3, MC9 and Alg3/MC9 hydrogel films was investigated (Fig. 4a). From the top view and side view, it could be seen that both Alg3 and MC9 contained porous structures wherein the pore size of Alg3 was larger than that of MC9. Blending of Alg3 and MC9 also remained the porous structure and its pore size looked like a combination of the big pore size of Alg3 and small pore size of MC9. Therefore, by using 4D printing, it is possible to fabricate heterogeneous Alg3/MC9 hydrogels by carefully controlling the difference of the porous degree at different regions of the hydrogels. In other words, the pore size gradient implies a network density gradient within the Alg3/MC9 hydrogels, resulting in anisotropic stiffness and swelling behavior of the printed architectures and hence shape morphing process upon immersion in $CaCl_2$ solution. As illustrated in Fig. 4b, the 4D printed three-layer Alg3/MC9 hydrogel can form the tightest networks at the three-layer areas due to their fusion and large compression during drying process at room temperature, resulting in the little porous and high dense regions. In contrast, the one-layer areas of the 4D printed Alg3/MC9 hydrogel can form relatively loose networks during drying process at room temperature, resulting in the high porous and sparse structures.

To further verify the shape morphing mechanism of the 4D printed Alg3/MC9 hydrogel, their microstructure was investigated under SEM, as shown in Fig. 4c. From the top view at the low magnification, it is seen that the 4D printed Alg3/MC9 patterned hydrogel exhibited dense regions at the printed three-layer part and sparse regions at the printed one-layer part. Besides, zoom images of the dense region revealed a non-porous structure, while that of the sparse region revealed a porous structure, indicating a difference of network density at these two regions. From the side view, the 4D printed Alg3/MC9 patterned hydrogels also revealed dense regions and sparse regions. Interestingly, the thickness of the three-layer part and one-layer part looked like the same, indicating that the printed three-layer part undergoes a large compression during drying at room temperature and hence generates little porous and highly dense regions. The dense regions with a high network density and fewer pores were rigid and had poor water absorption, while the sparse regions with a low network density and more pores exhibited good water absorption and a higher swelling degree when immersed in $CaCl_2$ solution. Therefore, the printed Alg3/MC9 hydrogel exhibits different swelling and stiffness properties at different regions (Fig. S5 and S6). Harnessing the anisotropic swelling allows precise control the deformation of 4D printed Alg3/MC9 architectures.

3.2.3. Fabrication of complex patterned hydrogels and their deformations

Printing of a hydrogel into complex structures with a high precision accuracy is generally challenging. In this work, with the excellent printability and shape morphing ability, Alg3/MC9 hydrogel can be 4D printed into a series of complex 3D morphologies. By combining patterns that generate different simple deformations, we designed and created a series of complex patterns which could change from 2D morphologies into complex 3D morphologies on immersion in 0.1 M $CaCl_2$ solution (Fig. 5). Inspired by the typical DNA molecular structures, a rectangle frame of Alg3/MC9 hydrogel was designed and printed with strips at the angle of 35°, and this architecture transformed into a perfect double helical structure (Fig. 5a, Movie S4 and S5). By combining of strips printed at 0°, 90°, 180° and 270° configurations in one Alg3/MC9 hydrogel pattern led to an open cage shape (Fig. 5b, Movie S6 and S7). These two shape morphing processes are vertical to the orientation of printed strips, indicating good preprogramming and smart design of these architectures.

Inspired by the flower opening/closing, we created five-petal flower patterns with each petal comprised of aligned strips with 0° or 45° configurations (Fig. 5c and d). As shown in Fig. 5c, the petals in the floral structure were composed of a 0° configuration and they could close vertically to the orientation of the strips when they swelled in 0.1 M $CaCl_2$ solution (Movie S8 and S9). Besides, when the petals in a floral structure were printed with strips at the angle of 45°, the resultant structure tended to be a twisted morphology as it swelled (Fig. 5d, Movie S10 and S11). To further demonstrate the versatility of the 3D printable and shape morphing Alg3/MC9 hydrogel, a highly complex orchid was designed by preprogramming multiple shape morphing domains. As shown in Fig. 5e, the resulting 3D morphology exhibited rolling, twisting and bending shape change when swelling in 0.1 M $CaCl_2$ solution (Movie S12), resembling the orchid structure.

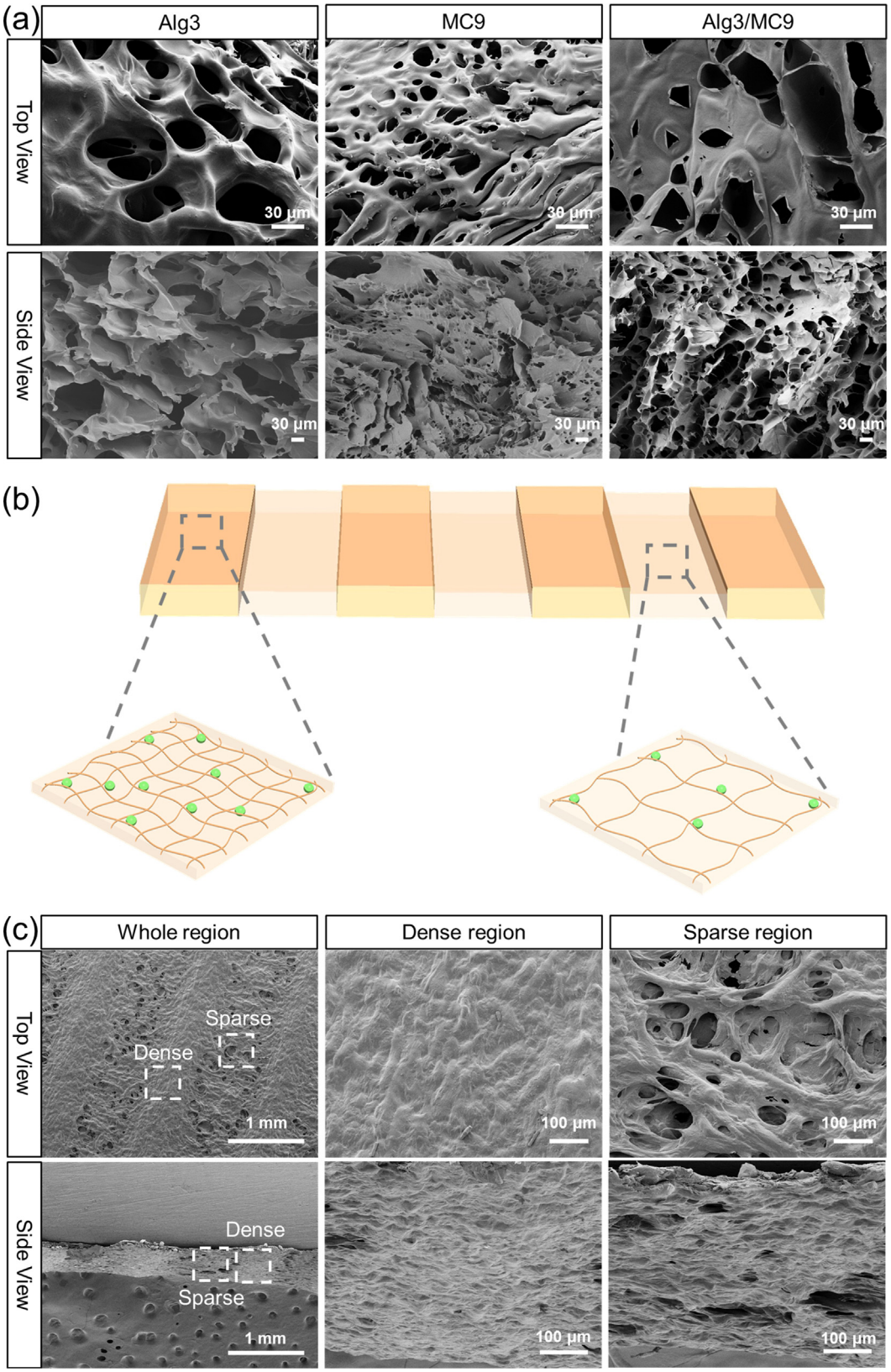

Fig. 4. (a) SEM images of the casted Alg3, MC9 and Alg3/MC9 hydrogel films with both top view and side view; (b) schematic illustration of the 4D printed Alg3/MC9 hydrogels with the difference of network density at different regions; (c) SEM images of the 4D printed Alg3/MC9 hydrogels with both top view and side view and zoom images of the dense region and sparse region with the top view and side view.

In recent years, a number of researchers have developed several pathways for preparing shape morphing hydrogels via 4D printing. Gladman *et al.* developed a hydrogel composite which was composed of N, N-dimethylacrylamide or poly(N-isopropylacrylamide) (PNIPAm), photoinitiator Irgacure 2959, nano clay Laponite XLG, nanofibrillated cellulose (NFC), glucose oxidase

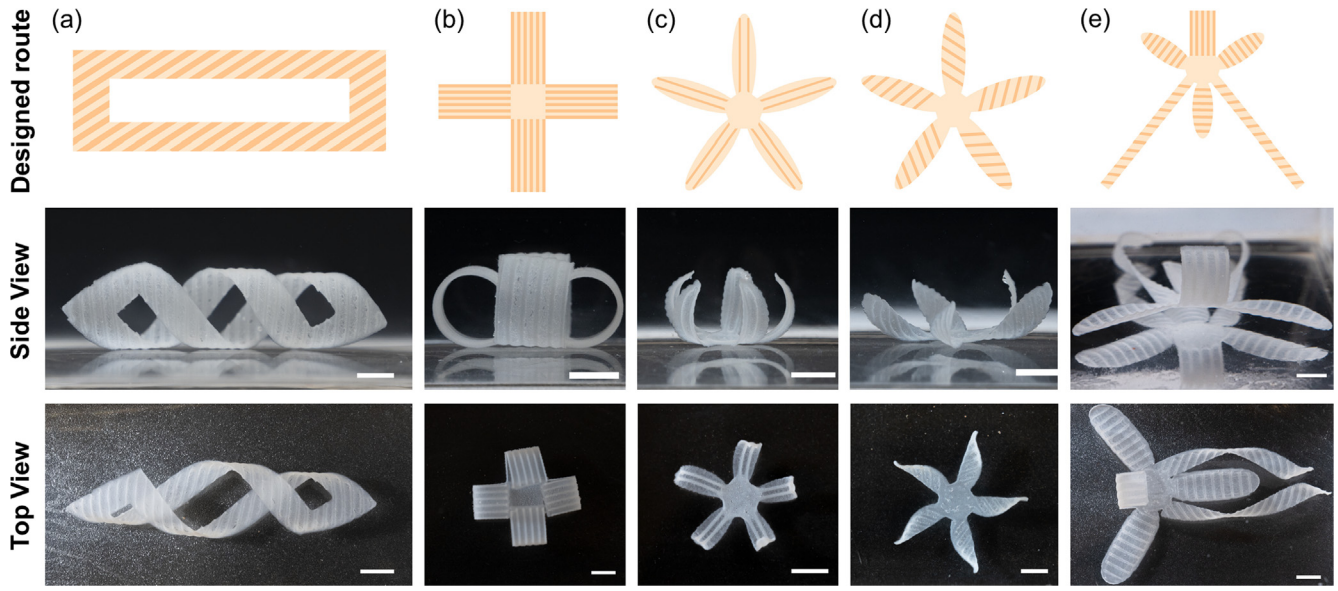

Fig. 5. Designed routes of the 4D printed patterned hydrogels and their corresponding 3D complex deformations from the side view and top view upon immersion in 0.1 M $CaCl_2$ solution: (a) a double helix with strip width of 1.4 mm and printing angle of 35°; (b) an open cage structure with strip width of 1.43 mm and printing angles of 0°, 90°, 180° and 270°; (c) a flower with each petal having strip width of 1.2 mm and printing angle of 0°; (d) a flower with each petal having strip width of 1.2 mm and printing angle of 45°; (e) an orchid with a top rolling petal having strip width of 1.84 mm and angle of 0°, three bending petals having strip width of 2 mm and angle of 90°, and two twisting petals having strip width of 2 mm and angle of 45° (Scale bar: 5 mm).

and glucose [25]. When the ink flowed through the nozzle, NFC was aligned due to the shear stress. The alignment of NFC led to anisotropic stiffness and swelling behaviour of the printed filaments in the longitudinal and transverse directions. By smartly designing the alignment patterns, they fabricated various plant-inspired bilayer architectures which could undergo 2D-to-3D shape transformations on immersion in water [25]. However, the hydrogel composite composition, preparation and the smart design in this work are complex and difficult. Liu *et al.* fabricated a variety of shape morphing structures by segmented printing of an active thermally responsive swelling gel (PNIPAm) and a passive thermally nonresponsive gel (polyacrylamide) [26]. Strategically placing segments of the swelling and nonswelling materials enabled the structures with 3D deformation of uniaxial elongation, radial expansion, bending, and gripping. However, multi-nozzle and multi-material printing require sophisticate and expensive 3D printers and more complex operation process than single material printing. Inspired by drying-driven curling of apple peels, single GelMA hydrogel flakes were printed, UV crosslinked, dried and then were re-swelling into various vascular structures with diameters of 50–500 μm [2]. The shape morphing degree was controlled by the concentration and crosslinking time of GelMA. But this work just demonstrated the simple tubular structures of shape morphing GelMA, which may be hard to print into more complex morphologies due to its relatively low printability. Kim *et al.* used digital light projection to process photocurable silk fibroin into various shape morphing bilayer structures by controlling the difference of photo crosslinking degree of each layer during printing [5]. However, these bilayer scaffolds required tens of minutes to complete the shape morphing process. In comparison, our developed strategy which was used to create shape morphing Alg3/MC9 hydrogels has following advantages: (1) simple material composition (i.e., aqueous solution containing Alg3 and MC9); (2) very easy and effective process to create the shape morphing hydrogels with anisotropic swelling (i.e., by controlling the strips width and angle of the printed three-layered architectures); (3) creation of heterogeneous dynamic structures without using chemical reactions; (4) excellent printability and printing accuracy, allowing the fabrication of both simple and complex architectures; (5) relatively fast shape morphing process with just a few minutes; (6) good biocompatibility and biodegradability of Alg3/MC9 hydrogel. To sum up, our study provides a facile method for 4D printing of printable and shape morphing Alg3/MC9 hydrogel, which is highly potential for a variety of biomedical applications such as tissue engineering and soft robotic devices. For example, the developed Alg3/MC9 hydrogels with shape morphing ability are beneficial for minimally- or non-invasive surgical implantation. The 4D printed Alg3/MC9 hydrogels can be packaged into small-size temporary shapes, which enables them to go through narrow passages to the target tissues, and then recover to their predesigned shapes after implantation. A demo of injection operation of a Alg3/MC9 hydrogel scaffold was shown in Fig. S7. The Alg3/MC9 hydrogel scaffold ($40 \times 20 \times 0.1$ mm^3) was compressed into a slender rod and then passed through a small tube via push with a glass stick. After injection, a fast shape recovery was occurred in $CaCl_2$ solution. 4D biofabrication using this hydrogel can also be expected. Cell-laden matrix or cell organoids may be bioprinted onto the dried Alg3/MC9 hydrogel to generate a cell-laden biphasic dynamic structure which can transform into predesigned structure upon immersion in $CaCl_2$ solution. Further exploration of the applications of the printable and shape morphing Alg3/MC9 hydrogel in the biomedical engineering field will be our future work.

4. Conclusions

In this study, a facile approach was developed to achieve 4D printing of Alg/MC hydrogels by controlling the network density gradient across the plane of the hydrogel architecture without using chemical reactions. The printability of Alg/MC hydrogels was investigated in terms of the rheological properties and shape fidelity. Alg3/MC9 hydrogel containing 3% (w/v) Alg and 9% (w/v) MC exhibited the best printability and could be printed into a series of simple and complex 2D patterns with high precision accuracy. Through the control of deformation parameters, which are as simple as strip width and orientation, these 2D patterns could undergo programmable deformations of simple 3D morphologies

such as rolling and helix or complex 3D morphologies such as double helix and flowers upon immersion in $CaCl_2$ solution. Owing to the excellent printability, biocompatibility and shape morphing ability of Alg3/MC9 hydrogels, our developed strategy shows highly potential for fabricating diverse dynamic architectures for biomedical engineering.

Declaration of Competing Interest

The authors declare that they have no known competing financial interests or personal relationships that could have appeared to influence the work reported in this paper.

Acknowledgements

J. Lai, J. Li and C. Wang thank The University of Hong Kong (HKU) for awarding them with PhD scholarships at HKU. This work was financially supported by Hong Kong Research Grants Council through a GRF research grant, Hong Kong, China (17201017), The Univeristy of Hong Kong through a Seed Fund for Basic Research grant, Dongguan University of Technology (KCYCXPT201603, TDYB2019003), Natural Science Foundation of Guangdong Province, China (2018A0303130019), Foundation and Applied Foundation Research Fund of Guangdong Province, China (No. 2019A1515110568), Natural Science Foundation of China (81801859, 81772428), Foundation Research Project of Shenzhen, China (JCYJ20180305125254860) and Department of Education of Guangdong Province, China (2016KQNCX163). Assistance provided by members in M. Wang's group and by technical staff in HKU's Department of Mechanical Engineering and Electron Microscopy Unit is acknowledged.

Appendix A. Supplementary material

Supplementary data to this article can be found online at https://doi.org/10.1016/j.matdes.2021.109699.

References

[1] C. Wang, H. Yue, W. Huang, X. Lin, X. Xie, Z. He, X. He, S. Liu, L. Bai, B. Lu, Y. Wei, M. Wang, Cryogenic 3D printing of heterogeneous scaffolds with gradient mechanical strengths and spatial delivery of osteogenic peptide/TGF-β1 for osteochondral tissue regeneration, Biofabrication 12 (2) (2020) 025030.
[2] L. Zhang, Y. Xiang, H. Zhang, L. Cheng, X. Mao, N. An, L. Zhang, J. Zhou, L. Deng, Y. Zhang, X. Sun, H.A. Santos, W. Cui, A biomimetic 3D-self-forming approach for microvascular scaffolds, Adv. Sci. 7 (9) (2020) 1903553.
[3] T. van Manen, S. Janbaz, A.A. Zadpoor, Programming 2D/3D shape-shifting with hobbyist 3D printers, Mater. Horiz. 4 (6) (2017) 1064–1069.
[4] M. Zarek, N. Mansour, S. Shapira, D. Cohn, 4D printing of shape memory-based personalized endoluminal medical devices, Macromol. Rapid Commun. 38 (2) (2017) 1600628.
[5] S.H. Kim, Y.B. Seo, Y.K. Yeon, Y.J. Lee, H.S. Park, M.T. Sultan, J.M. Lee, J.S. Lee, O.J. Lee, H. Hong, H. Lee, O. Ajiteru, Y.J. Suh, S.-H. Song, K.H. Lee, C.H. Park, 4D-bioprinted silk hydrogels for tissue engineering, Biomaterials 260 (2020) 120281.
[6] Z.X. Khoo, J.E.M. Teoh, Y. Liu, C.K. Chua, S. Yang, J. An, K.F. Leong, W.Y. Yeong, 3D printing of smart materials: a review on recent progresses in 4D printing, Virtual Phys. Prototyp. 10 (3) (2015) 103–122.
[7] J. Choi, O.C. Kwon, W. Jo, H.J. Lee, M.-W. Moon, 4D printing technology: A review, 3D Print. Addit. Manuf. 2 (4) (2015) 159–167.
[8] X. Kuang, D.J. Roach, J. Wu, C.M. Hamel, Z. Ding, T. Wang, M.L. Dunn, H.J. Qi, Advances in 4D printing: materials and applications, Adv. Funct. Mater. 29 (2) (2019) 1805290.
[9] J.W. Su, W. Gao, K. Trinh, S.M. Kenderes, E. Tekin Pulatsu, C. Zhang, A. Whittington, M. Lin, J. Lin, 4D printing of polyurethane paint-based composites, Int. J. Smart Nano Mater. 10 (3) (2019) 237–248.
[10] J. Lai, J. Li, M. Wang, 3D Printed porous tissue engineering scaffolds with the self-folding ability and controlled release of growth factor, MRS Commun. 10 (4) (2020) 579–586.
[11] C. Wang, H. Yue, J. Liu, Q. Zhao, Z. He, K. Li, B. Lu, W. Huang, Y. Wei, Y. Tang, M. Wang, Advanced reconfigurable scaffolds fabricated by 4D printing for treating critical-size bone defects of irregular shapes, Biofabrication 12 (4) (2020) 045025.
[12] A. Kirillova, R. Maxson, G. Stoychev, C.T. Gomillion, L. Ionov, 4D biofabrication using shape-morphing hydrogels, Adv. Mater. 29 (46) (2017) 1703443.
[13] J. Guo, R. Zhang, L. Zhang, X. Cao, 4D printing of robust hydrogels consisted of agarose nanofibers and polyacrylamide, ACS Macro Lett. 7 (4) (2018) 442–446.
[14] Z. Zhang, Y. Jin, J. Yin, C. Xu, R. Xiong, K. Christensen, B.R. Ringeisen, D.B. Chrisey, Y. Huang, Evaluation of bioink printability for bioprinting applications, Appl. Phys. Rev. 5 (4) (2018) 041304.
[15] A. Shafiee, E. Ghadiri, H. Ramesh, C. Kengla, J. Kassis, P. Calvert, D. Williams, A. Khademhosseini, R. Narayan, G. Forgacs, A. Atala, Physics of bioprinting, Appl. Phys. Rev. 6 (2) (2019) 021315.
[16] K.Y. Lee, D.J. Mooney, Alginate: properties and biomedical applications, Prog. Polym. Sci. 37 (1) (2012) 106–126.
[17] A. Eneko, L.O. Michelle, Applications of alginate-based bioinks in 3D bioprinting, Int. J. Mol. Sci. 17 (12) (2016) 1976.
[18] Y. Luo, X. Lin, B. Chen, X. Wei, Cell-laden four-dimensional bioprinting using near-infrared-triggered shape-morphing alginate/polydopamine bioinks, Biofabrication 11 (4) (2019) 045019.
[19] O. Eskens, G. Villani, S. Amin, Rheological investigation of thermoresponsive alginate-methylcellulose gels for epidermal growth factor formulation, Cosmetics 8 (1) (2021).
[20] H. Li, Y.J. Tan, K.F. Leong, L. Li, 3D Bioprinting of highly thixotropic alginate/methylcellulose hydrogel with strong interface bonding, ACS Appl. Mater. Interfaces 9 (23) (2017) 20086.
[21] K. Schütz, A.-M. Placht, B. Paul, S. Brüggemeier, M. Gelinsky, A. Lode, Three-dimensional plotting of a cell-laden alginate/methylcellulose blend: towards biofabrication of tissue engineering constructs with clinically relevant dimensions, J. Tissue Eng. Regen. Med. 11 (5) (2017) 1574–1587.
[22] H. Li, S. Liu, L. Li, Rheological study on 3D printability of alginate hydrogel and effect of graphene oxide, Int. J. Bioprinting 2 (2) (2016) 54–66.
[23] Z.L. Wu, M. Moshe, J. Greener, H. Therien-Aubin, Z. Nie, E. Sharon, E. Kumacheva, Three-dimensional shape transformations of hydrogel sheets induced by small-scale modulation of internal stresses, Nat. Commun. 4 (1) (2013) 1–7.
[24] X. Du, H. Cui, Q. Zhao, J. Wang, H. Chen, Y. Wang, Inside-out 3D reversible ion-triggered shape-morphing hydrogels, Research 2019 (2019) 6398296.
[25] A.S. Gladman, E.A. Matsumoto, R.G. Nuzzo, L. Mahadevan, J.A. Lewis, Biomimetic 4D printing, Nat. Mater. 15 (4) (2016) 413.
[26] J. Liu, O. Erol, A. Pantula, W. Liu, Z. Jiang, K. Kobayashi, D. Chatterjee, N. Hibino, L.H. Romer, S.H. Kang, T.D. Nguyen, D.H. Gracias, Dual-gel 4D printing of bioinspired tubes, ACS Appl. Mater. Interfaces 11 (8) (2019) 8492–8498.